Applied Catalysis B: Environmental 179 (2015) 285–291

Contents lists available at ScienceDirect

Applied Catalysis B: Environmental

journal homepage: www.elsevier.com/locate/apcatb

Development of electrodeposited IrO_2 electrodes as anodes in polymer electrolyte membrane water electrolysis

Byung-Seok Lee[a,b], Sang Hyun Ahn[a], Hee-Young Park[a], Insoo Choi[a], Sung Jong Yoo[a], Hyoung-Juhn Kim[a], Dirk Henkensmeier[a], Jin Young Kim[a], Sehkyu Park[d], Suk Woo Nam[a,c], Kwan-Young Lee[b,c,**], Jong Hyun Jang[a,c,*]

[a] Fuel Cell Research Center, Korea Institute of Science and Technology (KIST), Hwarangno 14-gil 5, Seongbuk-gu, Seoul 136-791, Republic of Korea
[b] Department of Chemical and Biological Engineering, Korea University, 145, Anam-ro, Seongbuk-gu, Seoul 136-701, Republic of Korea
[c] Green School, Korea University, 145, Anam-ro, Seongbuk-gu, Seoul 136-701, Republic of Korea
[d] Department of Chemical Engineering, Kwangwoon University, 20,Gwangun-ro, Nowon-gu, Seoul 139-701, Republic of Korea

ARTICLE INFO

Article history:
Received 27 January 2015
Received in revised form 7 May 2015
Accepted 12 May 2015
Available online 14 May 2015

Keywords:
Polymer electrolyte membrane water electrolysis
Iridium oxide
Electrodeposition
Oxygen evolution reaction
Single cell test

ABSTRACT

To reduce the use of noble metals, iridium oxide (IrO_2) catalysts are prepared on carbon paper (CP) by electrodeposition for use as the anodes in polymer electrolyte membrane water electrolysis (PEMWE). The activities of the fabricated electrodes toward the oxygen evolution reaction are evaluated. The loading amount and morphology of the IrO_2 deposits are varied by controlling the electrodeposition potential (E_{dep}) and time (t_{dep}). When electrodeposited at 0.7 V, the IrO_2 loading ranges from 0.007 to 0.464 mg cm^{-2} (t_{dep}: 1 ~ 30 min). In the PEMWE test at 90 °C, the IrO_2/CP electrode with an IrO_2 loading of 0.1 mg cm^{-2} shows the highest performance (1.92 A cm^{-2} at 1.8 V) in which high IrO_2 utilization is achieved without significant exposure of the substrate carbon surface. The developed IrO_2/CP electrodes provide cell performances comparable to those in previous reports with a higher IrO_2 loading, indicating markedly enhanced mass activity.

1. Introduction

Due to global climate change and the limited reserves of fossil fuels, the idea of transition to a hydrogen economy has recently gained significant attention. Hydrogen possesses many advantages as an alternative energy source because it does not produce any pollutants and can be stored in either small or large quantities for long periods without significant losses [1–3]. Currently, hydrogen is primarily produced by steam reforming of natural gas [4–8], in which a significant amount of CO_2 is produced. As a sustainable and environmentally friendly alternative, water electrolysis combined with renewable electricity sources, such as wind and solar power, is expected to provide a practical solution for the production of hydrogen. However, hydrogen production by water electrolysis is at least two to three times more expensive than steam reforming [9]. Currently, approximately 96% of hydrogen is produced by fossil fuel-based technologies, such as reforming of natural gas (48%), partial oxidation (30%), and gasification of coal (18%), whereas, only 4% of the total hydrogen production is produced by water electrolysis [10,11].

Among several types of water electrolysis technologies, polymer electrolyte membrane water electrolysis (PEMWE) has many advantages, such as high purity of produced hydrogen (greater than 99.99%), high production rate and small volume of the system, as well as being ecologically harmless due to the use of neutral water [12–14]. In typical PEMWE, iridium- and ruthenium-based electrocatalysts are utilized for the oxygen evolution reaction (OER) at the anodes (1.0–5.0 mg cm^{-2}), and platinum is used for the hydrogen evolution reaction (HER) at the cathodes (0.4–0.8 mg cm^{-2}) [15–21]. These noble metal-based electrocatalysts constitute a significant portion of the high system cost of PEMWE. However, it has been reported that the single cell performances significantly decreased when the Ir or IrO_2 loading was decreased to levels below 1.0 mg cm^{-2} in the PEMWE membrane electrode assembly (MEA) fabricated by the spraying method [12,22] and the sputtering method [23–25]. For example, Su et al. [22] have reported that the current density at 1.6 V gradually decreased from 1.33 to 0.67 A cm^{-2} as the IrO_2 loading decreased from 3.0 mg cm^{-2} to 0.5 mg cm^{-2} (spraying method). Certain studies have also devel-

* Corresponding author. Tel.: +82 2 9585287; fax: +82 2 9585199.
** Corresponding author. Tel.: +82 2 32903299; fax: +82 2 9266102.
E-mail address: jhjang@kist.re.kr (K.-Y. Lee).

http://dx.doi.org/10.1016/j.apcatb.2015.05.027
0926-3373/

oped Ir-based mixed oxides [26–28] and an oxide mixture [29]. In PEMWE single cell tests, enhanced performances compared with IrO_2 have been reported for $Ir_xRu_yO_2$ (2.0 mg cm^{-2}) [28], whereas, the Sn doping resulted in a decreased activity [27].

Previously, the electrodeposition method has been utilized to fabricate the MEA. It has been reported that the loading amount of the Pt and Ni electrocatalysts could be significantly reduced with no significant performance loss for the PEM-based fuel cell (PEMFC) [30,31] and the anion exchange membrane-based water electrolyzer (AEMWE) [32], respectively. The electrodeposition method has also been utilized to prepare iridium oxide films as an electrochromic material on various substrate materials, such as indium-tin oxide (ITO) [33], poly (*p*-phenylene terephthalamide) [34], or boron-doped diamond [35], platinum [36–39], titanium [38] and gold [38,40,41].

In this study, for use as the anodes in PEMWE, the IrO_2 electrodes were fabricated by electrodeposition on carbon papers (CP), which are expected to provide a reduced metal loading (higher utilization) and a simple fabrication process. The effects of electrodeposition parameters, such as potential and time, on the IrO_2 loading and microstructure were investigated. Then, PEMWE MEAs were prepared with the fabricated IrO_2/CP electrodes, and the single cell performances were evaluated. The polarization characteristics were discussed, and the mass activities were compared with previous reports to suggest potential applications of the electrodeposited IrO_2/CP with reduced IrO_2 loading in PEMWE.

2. Experimental

2.1. Fabrication of IrO_2/CP electrodes by anodic electrodeposition

To prepare the electrodeposition solution, 0.1 M iridium chloride hydrate ($IrCl_4{\cdot}H_2O$) was dissolved in deionized water (DI water) and mixed for 30 min under magnetic stirring. Then, oxalic acid ($(COOH)_2{\cdot}2H_2O$:5 g L^{-1}) and hydrogen peroxide (35% H_2O_2:10 g L^{-1}) were added, and the resulting solution was mixed for 10 min. After the solution pH was adjusted to 10.5 by the addition of anhydrous potassium carbonate, the electrodeposition solution was stirred for 3 days to allow stabilization.

The anodic electrodeposition was performed using a three-electrode electrochemical cell in which a SIGNADUR® glassy carbon rod electrode (diameter: 4 mm, HTW Germany) and a saturated calomel electrode (SCE, Hanna instruments Ltd.) were used as the counter and reference electrodes, respectively. CP (thickness: 280 μm, TGPH-090, Toray Inc.) was placed at the bottom of the electrodeposition cell. The deposition potential was applied to the CP through aluminum foil using a potentiostat (AUT302N, AUTO LAB Ltd.). Linear sweep voltammetry (LSV) was performed in the deposition solution from 0.2 V to 1.4 V with a scan rate of 50 mV s^{-1}. The IrO_2 electrodeposition was conducted by applying constant potentials (0.6 V ~ 0.9 V) for various deposition times (1 ~ 30 min).

2.2. Characterization of the IrO_2/CP electrodes

Cyclic voltammetry (CV) was performed in a 0.1 M $HClO_4$ solution from −0.5 V to 1.5 V at a scan rate of 5 mV s^{-1} (AUT302N, AUTO LAB Ltd.). The morphologies and elemental compositions of the IrO_2/CP electrodes were analyzed by scanning electron microscopy (SEM) (Inspect F50, Field emission Inc. and S-4100, Hitachi Ltd.) and inductively coupled plasma mass spectrometry (ICP-MS, iCAP 6300 series, Thermo Ltd.), respectively. Additionally, the composition of the deposits was analyzed by X-ray photoelectron spectroscopy (XPS, PHI 5000 VersaProbe, Ulvac-PHI Ltd.) using Al Kα (1486.6 eV) radiation.

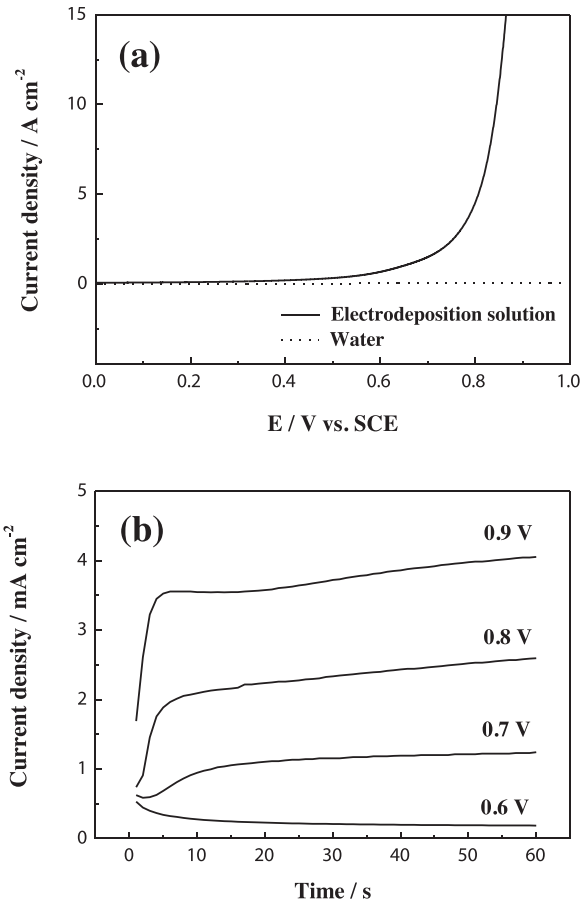

Fig. 1. (a) linear sweep voltammetry curves for the CP electrodes in the electrodeposition solution and pH adjusted water, and (b) current density during the electrodeposition under a constant potential of 0.6 V, 0.7 V, 0.8 V and 0.9 V.

2.3. PEMWE single cell test with IrO_2/CP anodes

The PEMWE single cells were fabricated by placing the IrO_2/CP anodes and the Pt/C cathodes with the GDL (thickness: 280 μm, 5% PTFE, 10 BC, SGL group) on two sides of Nafion 212 membranes (thickness: 50 μm, DuPont Co.). The Pt/C cathodes were prepared on 10 BC (SGL carbon Ltd.) by spraying catalyst inks, which were prepared by mixing 46.3% Pt/C (TKK) and DI water, followed by the addition of isopropanol and 5 wt% Nafion ionomer (DuPont Co.). The active area was 4 cm^2, and the Pt loading at the cathodes was fixed at 0.4 mg cm^{-2}. After cell assembly, the cell temperature was raised to 90 °C, and polarization analysis for water electrolysis was conducted (HCP-803, Biologics Ltd.). Using a pre-heated DI water feed to the anode (15 mL min^{-1}), stabilized currents were applied at various cell voltages from 1.35 V to 2.0 V with an interval of 0.05 V.

3. Results and discussion

Fig. 1a shows the LSV result for a CP electrode in the electrodeposition solution, which contains 0.1 M iridium chloride hydrate, 0.04 M oxalic acid, and 0.01 M hydrogen peroxide [33]. When the electrode potential was swept anodically from 0 V (scan rate: 50 mV s^{-1}), the anodic current appeared at ca. 0.3 V, gradually increased with further polarization, and increased rapidly at ca. 0.8 V. In the electrodeposition solution, the anodic currents can be ascribed to the electrochemical oxidation of the ligand in the Ir complex, resulting in the formation of CO_2 and IrO_2 [33], and to the

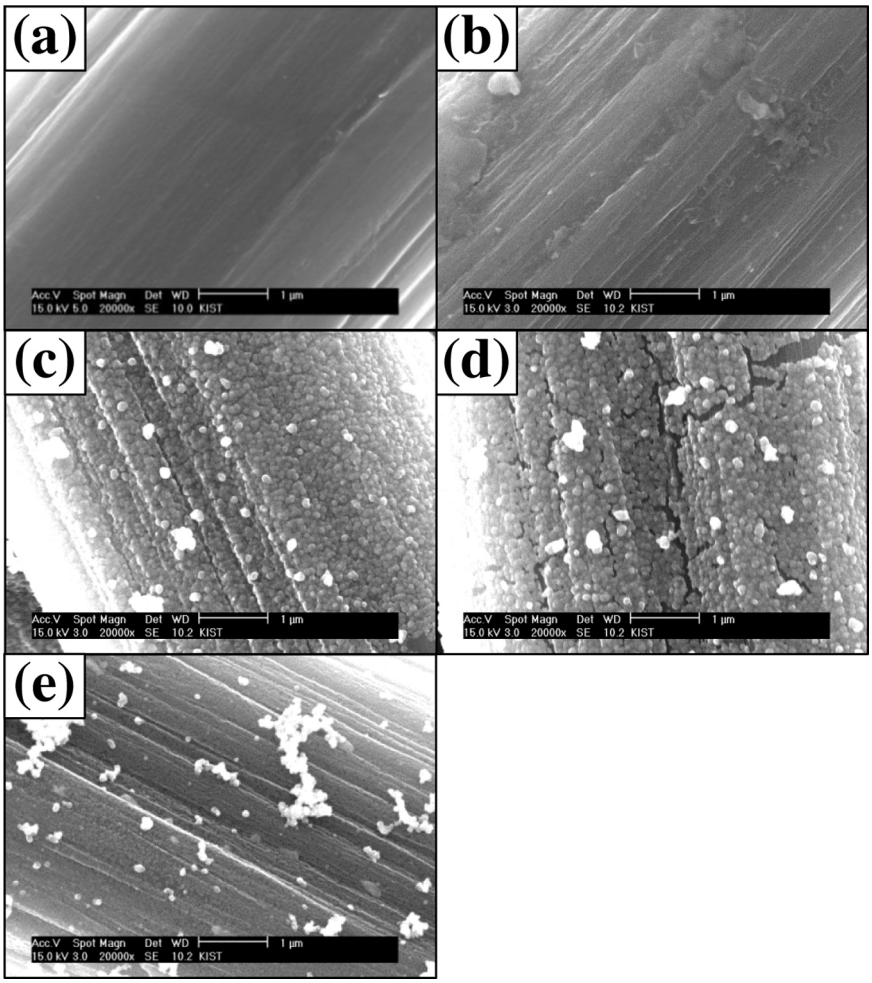

Fig. 2. The SEM images of (a) bare carbon paper and the IrO_2/CP electrodes fabricated by electrodeposition with an electrodeposition potential of (b) 0.6 V, (c) 0.7 V, (d) 0.8 V and (d) 0.9 V. The electrodeposition time was 60 s for the IrO_2/CP electrodes.

OER on the electrodeposited IrO_2 [42]. In the case of water with a similar pH (pH of 10.5), no significant current was observed.

$$[Ir(COO)_2(OH)_4]^{2-} \rightarrow IrO_2 + 2CO_2 + 2H_2O + 2e^- \quad (1)$$

The anodic electrodeposition was performed at various electrodeposition potentials (E_{dep}) (0.6 ~ 0.9 V) for 60 s. As shown in Fig. 1b, the current density gradually increased with a more positive potential (larger anodic overpotential) in which the current densities after 60 s were 0.2 mA cm^{-2} (0.6 V) → 1.2 mA cm^{-2} (0.7 V) → 2.5 mA cm^{-2} (0.8 V) → 3.8 mA cm^{-2} (0.9 V). However, the current density (or anodic charge) at each deposition potential cannot be directly correlated with the amount of the IrO_2 deposition because oxygen evolution can also occur over the potential range. When OER is also significant, it is expected that the produced oxygen bubbles could block the surface of the electrodeposited IrO_2 and even physically detach the IrO_2 thin film.

Compared with the initial surface morphology of CP (Fig. 2a), there were no significant morphological changes at a deposition potential of 0.6 V (Fig. 2b), at which only a small number of adsorbed particles was observed. When the electrodeposition potential was increased to 0.7 V (Fig. 2c), the amount of IrO_2 deposits increased markedly, consistent with the significant current increase as the deposition potential increased from 0.6 V to 0.7 V. At an anodic potential of 0.8 V (Fig. 2d), the morphology of the IrO_2-covered parts was similar to that at an anodic potential of 0.7 V, but many cracks were found in the electrodeposited IrO_2 layer. When the deposition potential was increased to 0.9 V, the surface coverage of the IrO_2 particles markedly decreased (Fig. 2e), although the total current density was the highest in this case, suggesting that the IrO_2 deposition was severely hindered by rapid oxygen evolution.

For a sample prepared by electrodeposition at 0.7 V for 5 min, X-ray photoelectron spectroscopy (XPS) analysis was performed; the binding energy region of Ir4f is presented in Fig. 3. The major peaks were observed at approximately 65.4 eV and 62.5 eV of binding energy, which are assigned to $4f_{5/2}$ and $4f_{7/2}$, respectively. From the

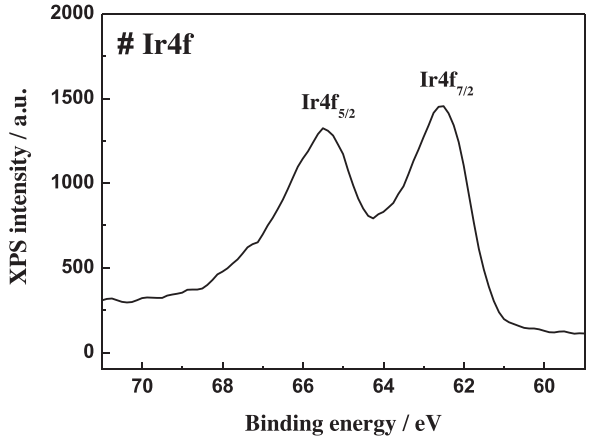

Fig. 3. Ir4f X-ray photoelectron spectra of electrodeposited IrO_2 on carbon paper.

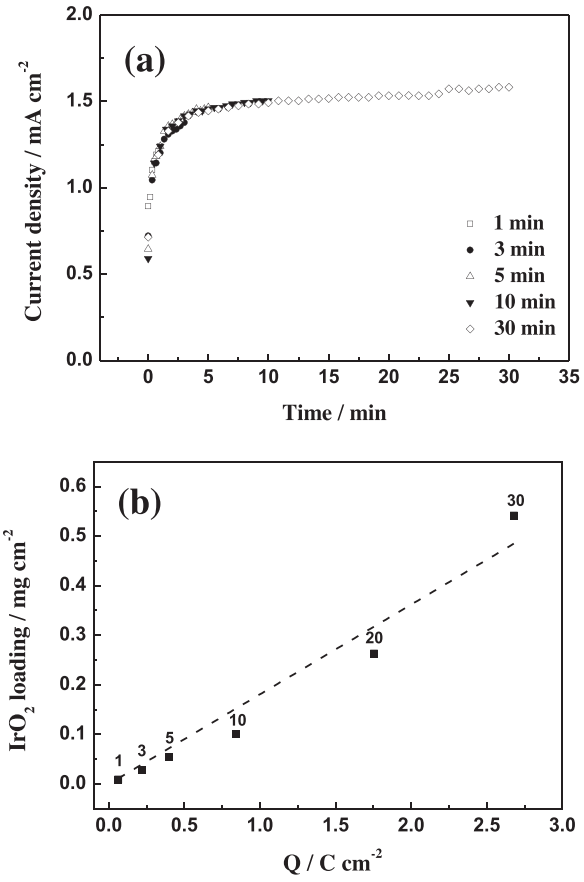

Fig. 4. (a) current density during electrodeposition at 0.7 V for various electrodeposition times from 1 min to 30 min, and (b) IrO_2 amount as a function of electrical charge for electrodeposition.

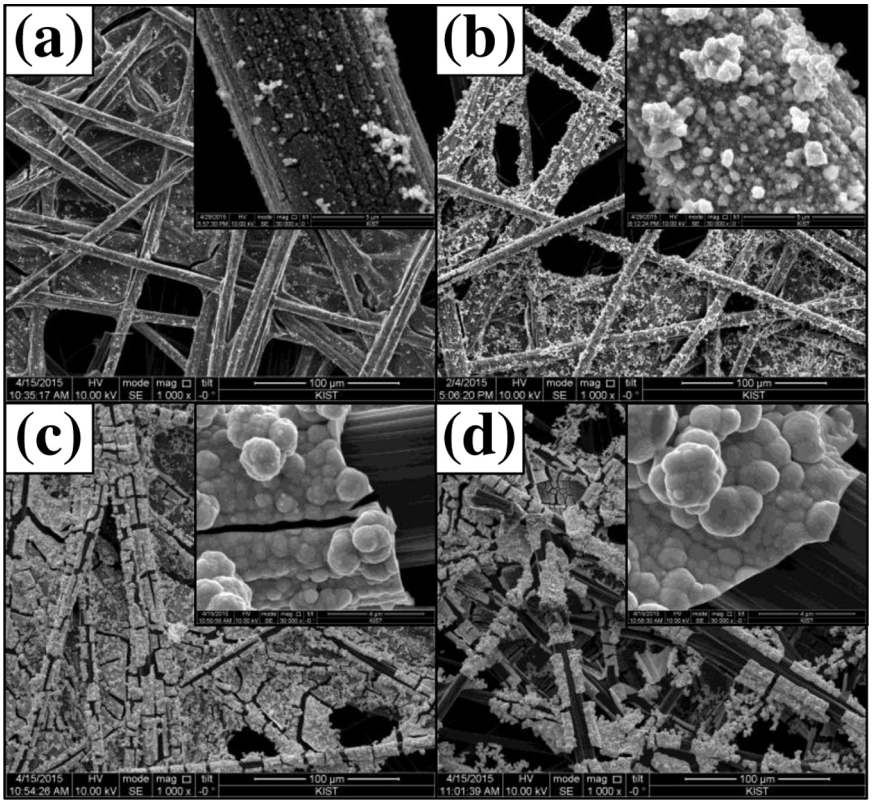

Fig. 5. SEM images of the IrO_2/CP electrodes fabricated by electrodeposition at 0.7 V for (a) 1 min, (b) 10 min, (c) 20 min, and (d) 30 min.

peak position, the deposits developed by electrodeposition could be confirmed as IrO_2 because it has been previously reported that the $Ir4f_{7/2}$ of IrO_2 appeared at 62.0 ~ 63.7 eV [10,34,42–45] and that of the Ir metal appeared at 60.6 eV [46] and 61.0 eV [43,44].

The E_{dep} was fixed at 0.7 V, and the effect of the deposition time (t_{dep}) was investigated (1 min ~ 30 min). Fig. 4a shows that the electrodeposition was reproducible; the anodic current density initially increased and stabilized after 5 min at ca. 1.5 mA cm^{-2}. The amount of catalyst deposited on CP with various deposition times was analyzed by ICP, and the resultant IrO_2 loading amounts were plotted as a function of the integrated electrical charge density (Fig. 4b). As the deposition time increased, the loading amount linearly increased up to 0.541 mg cm^{-2} (t_{dep} = 30 min). If the anodic current was utilized only to form IrO_2, then the slope in IrO_2 loading vs. electrical charge is expected to be 0.181 C mg^{-1}. However, when the experimental data points were analyzed using linear regression, the slope was 0.181 mg C^{-1}, indicating that the apparent coulombic efficiency of the IrO_2 deposition is approximately 15.6%. This result suggests that the oxygen evolution is also significant at the deposition potential of 0.7 V. In addition, the IrO_2 that was electrodeposited with charge consumption can be detached, especially under severe oxygen evolution.

Fig. 5shows the morphology of the IrO_2/CP electrodes electrodeposited at various deposition times. After 1 min of electrodeposition, IrO_2 deposits were observed on most part of CP surface, but crack-like uncovered region could be also detected. When the deposition time was increased to 10 min, a large number of spherical particles developed, suggesting an increased surface area of IrO_2. As the deposition time further increased, the particle size gradually increased from ca. 0.7 μm (t_{dep} = 10 min) to 1.7 μm (t_{dep} = 30 min), and more cracks developed, exposing the bare carbon surface as previously reported [47,48].

Fig. 6a shows the CV curves of the IrO_2/CP electrodes in a 0.1 M $HClO_4$ solution. For the sample with the smallest IrO_2 loading (t_{dep} = 1 min), anodic (0.8 V and 1.15 V) and cathodic (0.75 V) peaks for the Ir(III)/Ir(IV) redox are clearly observed (Fig. 6a, inset), which is in accordance with a previous report [49]. Regarding the Ir(IV)/Ir(V) redox pair, which is active only for surface atoms, the cathodic peak appears at 1.35 V, but the corresponding anodic peak overlaps markedly with the OER peak. Therefore, the intensity of the cathodic peak at 1.3 ~ 1.1 V was utilized to estimate the variation of the IrO_2 active area (Fig. 6b). The cathodic current density linearly increased with the IrO_2 loading for a deposition time of up to 10 min. However, with further IrO_2 loading (t_{dep}: 20 and 30 min), the increase of the peak current density decelerated, indicating that the IrO_2 utilization is lower, as expected from the larger particle sizes in the SEM images. Note that when the cathodic peaks are overlapped (t_{dep} = 20 and 30 min), the measured peak current will be higher than the actual current for Ir(IV)/Ir(V). In addition, IrO_2/CP samples with t_{dep} of 20 and 30 min showed a negative shift of the cathodic peak potential, which suggests more intensive overlapping by the bulk reduction of Ir(IV) to Ir(III) as the particle size increases.

Using the IrO_2/CP electrodes with various IrO_2 loadings as anodes, single cells were fabricated, and their water electrolysis performances were evaluated. For every cell, the cathodes were fabricated by spraying catalyst inks (commercial Pt/C and ionomer) onto CP. Fig. 7 shows polarization curves at 90 °C. As the deposition time increased up to 10 min, the current densities gradually increased, most likely due to the higher catalytic activities toward the oxygen evolution reaction. When the IrO_2 loading amount further increased (t_{dep} > 10 min), the current density at a low cell voltage (<1.5 V) continued to increase, but the performance at typical operating voltages (1.8–2.0 V [15]) relatively decreased. Typical behavior from activation overptential, which is related to the electron transfer, could be observed at low current density region. As

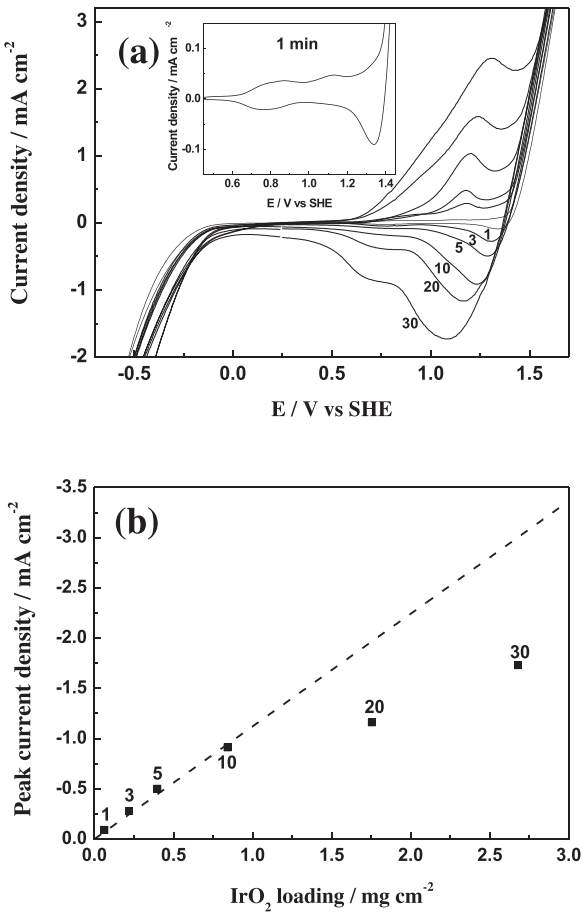

Fig. 6. (a) cyclic voltammogram and (b) peak current density of the Ir(V) reduction as a function of IrO_2 loading in which the electrodeposition time was indicated for the IrO_2/CP electrodes electrodeposited at 0.7 V.

the current density was increased from OCV condition, the applied cell voltage increased rapidly, and the increase rate became gradually slowed down (~ca. 0.4 A cm^{-2}). The IrO_2/CP anode with t_{dep} of 1 min showed the largest cell voltage increase at low current density (~ca. 0.1 A cm^{-2}), indicating that the amount of electrocatalyst is not sufficient; its current density decreased with voltage increase (>1.7 V), probably due to the CP corrosion that are exposed between IrO_2 deposits as shown in Fig. 5a. For IrO_2/CP anodes with

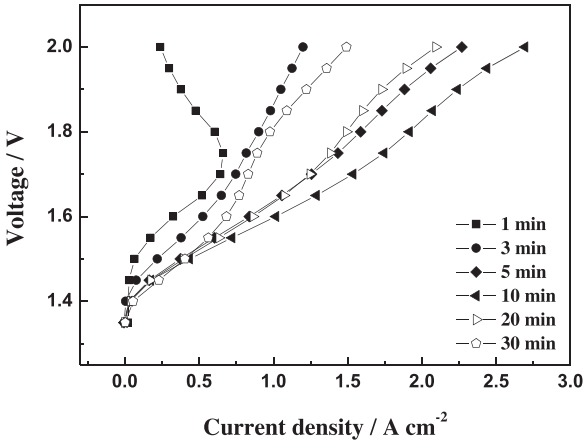

Fig. 7. Polarization curves of the PEMWE single cells with IrO_2/CP anodes (E_{dep} = 0.7 V; t_{dep} = 1 ~ 30 min).

Table 1
Summary of PEM water electrolysis described in the literature. The numbers in parenthesis indicate the anode loading (anode and current density) or cathode loading (cathode) in mg cm^{-2}

	MEA fabricationmethod	Anode	Cathode	Membrane	T (°C)	i@ 1.6 V(A cm^{-2})
A. Marshall et al. [28]	Spraying	IrO_2 (2.0)	Pt/C (0.4)	N115	80	0.75
S. Song et al. [51]	Spraying	Ir, IrO_2 (3.0)	Pt/C (0.5)	N112	80	0.52
J. Cheng et al. [50]	Spraying	IrO_2 (1.5)	Pt/C (0.5)	N1035	80	0.68
L. Ma et al. [12]	Brushing	Ir (1.5)	Pt (1.0)	N112	80	0.5
G. Wei et al. [10]	Decal	Ir (3.8)	Pt (2.3)	N112	60	0.25
H. Su et al. [22]	Spraying	IrO_2 (0.5~4.0)	Pt/C (0.5)	N212	80	1.32 (3.0)
E. Slavcheva et al. [23]	Sputtering	IrO_2 (0.2)	Pt/C (N.A.)	N117	80	0.3
This study	Electrodeposition	IrO_2 (0.01~0.54)	Pt/C (0.4)	N112	90	1.01 (0.1)

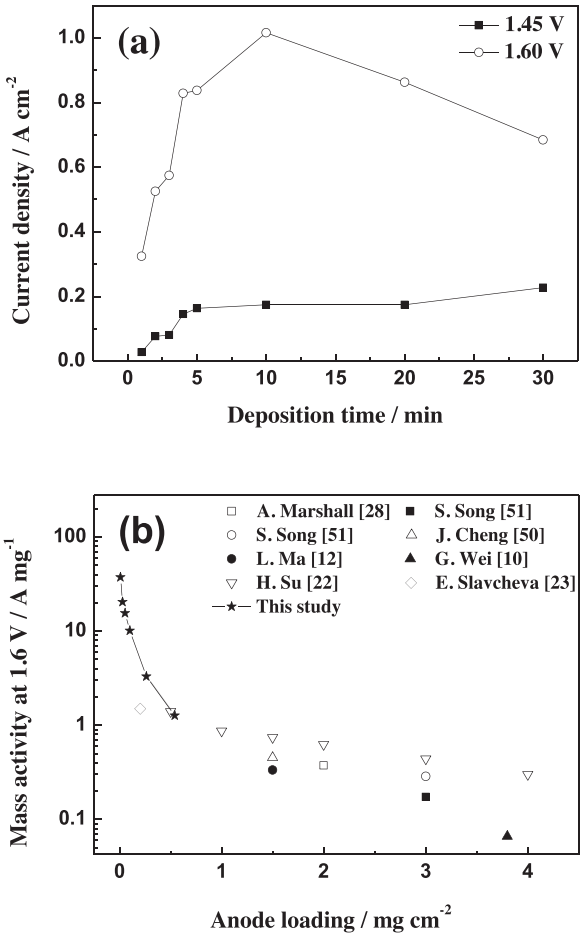

Fig. 8. (a) current density at 1.45 V (closed circles) and 1.60 V (open circles) and mass activity at 1.6 V as a function of anode loading.

t_{dep} of 10 min, the current density gradually increased with higher cell voltage up to 2.0 V, where, the ohmic drops is significant.

Fig. 8a shows the current densities at 1.45 V and 1.60 V, which correspond to the kinetic region and practical operating voltage, respectively. At 1.45 V, the performances are primarily determined by activation overpotentials, and it can be observed that the performance at a low overpotential rapidly increased with the loading amount up to a deposition time of 5 min. However, a deposition time longer than 5 min provided a relatively small enhancement in the performances, indicating that the utilization of IrO_2 was reduced. The current density at 1.6 V showed a maximum at an IrO_2 loading of 0.1 mg cm^{-2} (t_{dep} = 10 min). When the deposition time is longer than 10 min, it appears that carbon substrates exposed between the IrO_2 deposits are degraded at high operating voltages. The effect of carbon corrosion can be more clearly observed for the single cell with the smallest IrO_2 loading (t_{dep} = 1 min). Therefore, it can be concluded that it is very important to avoid carbon exposure, through either low IrO_2 loading or crack formation with high loading, to achieve high cell performances with good catalytic activity and low carbon corrosion.

The PEMWE performances with the electrodeposited IrO_2/CP electrodes in this study were compared with previous reports with IrO_2 [22,23,28,50,51] and iridium black [10,12] anodes (Table 1). Previously, the current density at 1.6 V has been reported as ranging from 0.25 to 1.32 A cm^{-2} with high Ir or IrO_2 loading (1.5 ~ 3.0 mg cm^{-2}). Therefore, the PEMWE performance of the electrodeposited IrO_2/CP in this study (1.01 A cm^{-2} at 1.6 V) appears promising, even though the IrO_2 loading was decreased to 0.1 mg cm^{-2}. The current density at 1.6 V was divided by the anode loading, and the resultant mass activity (MA) is presented in Fig. 8b. For previous reports by various authors, a gradual MA increase with a smaller loading can be observed, while the submicron anode loading provided an enhanced MA of 1.4 A mg^{-1} (0.5 mg cm^{-2}) [22] and 1.5 A mg^{-1} (0.2 mg cm^{-2}) [23]. The IrO_2/CP with an IrO_2 loading of 0.03 mg cm^{-2} showed an MA of 20.4 A mg^{-1}, which provided stable cell performances.

4. Conclusions

The IrO_2/CP electrodes were fabricated by anodic electrodeposition with various deposition voltages and times in which the evolution of the morphology and the Coulombic efficiency were analyzed by SEM, ICP, and CV. Spherical particles of IrO_2 were obtained by electrodeposition at 0.7 V for 10 min (0.1 mg cm^{-2}), whereas, a higher deposition voltage or longer time induced cracks that exposed the substrate carbon. In the PEMWE single cell test, the current density at 1.6 V was as high as 1.01 A cm^{-2}, which is comparable to previous reports with a higher anode loading (> 1.5 mg cm^{-2}). Additionally, enhanced mass activity could be confirmed, suggesting the possible application of IrO_2/CP for PEMWE with reduced material costs.

Acknowledgements

This study was supported by the Korean Government through the New and Renewable Energy Core Technology Program of the Korea Institute of Energy Technology Evaluation and Planning (KETEP) funded by MOTIE (No. 20133030011320), the Korea CCS R&D Center (KCRC) grant funded by MSIP (No. 2014M1A8A1049349), the National Research Foundation of Korea Grant funded by MSIP (2014, University-Institute cooperation program), and the Global Frontier R&D Program at the Center for Multiscale Energy System funded by the National Research Foundation, MSIP (No. 2012M3A6A7054283). This work was also financially supported by KIST through Institutional Projects (2E25411 and 2E25420).

References

[1] F. Muellerlanger, E. Tzimas, M. Kaltschmitt, S. Peteves, Int. J. Hydrogen Energy 32 (2007) 3797–3810.
[2] U. Bossel, B. Eliasson, G. Taylor, Cogener. Distr. Gener. J. 18 (2003) 29–70.
[3] O. Bičáková, P. Straka, Int. J. Hydrogen Energy 37 (2012) 11563–11578.
[4] Y. Bang, J.G. Seo, M.H. Youn, I.K. Song, Int. J. Hydrogen Energy 37 (2012) 1436–1443.
[5] J.G. Seo, M.H. Youn, K.M. Cho, S. Park, I.K. Song, J. Power Sources 173 (2007) 943–949.
[6] Y. Chen, Y. Wang, H. Xu, G. Xiong, Appl. Catal. B: Environ. 81 (2008) 283–294.
[7] U. Izquierdo, V.L. Barrio, J.F. Cambra, J. Requies, M.B. Guemez, P.L. Arias, G. Kolb, R. Zapf, A.M. Gutierrez, J.R. Arraibi, Int. J. Hydrogen Energy 37 (2012) 7026–7033.
[8] H.-S. Roh, K.Y. Koo, U.H. Jung, W.L. Yoon, Curr. Appl. Phys. 10 (2010) S37–S39.
[9] A.Q.E. Pham See, D. Lenz, P. Martin, R. Glass, Proceedings of the 2002 US DOE Hydrogen Program Review (2000).
[10] G. Wei, Y. Wang, C. Huang, Q. Gao, Z. Wang, L. Xu, Int. J. Hydrogen Energy 35 (2010) 3951–3957.
[11] Hysafe, Biennial Report on Hydrogen Safety, Biennial Report on Hydrogen Safety, 2006.
[12] L. Ma, S. Sui, Y. Zhai, Int. J. Hydrogen Energy 34 (2009) 678–684.
[13] S.A. Grigoriev, P. Millet, S.A. Volobuev, V.N. Fateev, Int. J. Hydrogen Energy 34 (2009) 4968–4973.
[14] S.A. Grigoriev, V.I. Porembsky, V.N. Fateev, Int. J. Hydrogen Energy 31 (2006) 171–175.
[15] M. Carmo, D.L. Fritz, J. Mergel, D. Stolten, Int. J. Hydrogen Energy 38 (2013) 4901–4934.
[16] V. Baglio, R. Ornelas, F. Matteucci, F. Martina, G. Ciccarella, I. Zama, L.G. Arriaga, V. Antonucci, A.S. Aricò, Fuel Cells 9 (2009) 247–252.
[17] J. Xu, G. Liu, J. Li, X. Wang, Electrochim. Acta 59 (2012) 105–112.
[18] S. Siracusano, V. Baglio, N. Briguglio, G. Brunaccini, A. Di Blasi, A. Stassi, R. Ornelas, E. Trifoni, V. Antonucci, A.S. Aricò, Int. J. Hydrogen Energy 37 (2012) 1939–1946.
[19] S.A. Grigoriev, M.S. Mamat, K.A. Dzhus, G.S. Walker, P. Millet, Int. J. Hydrogen Energy 36 (2011) 4143–4147.
[20] G. Wei, L. Xu, C. Huang, Y. Wang, Int. J. Hydrogen Energy 35 (2010) 7778–7783.
[21] V. Antonucci, A. Di Blasi, V. Baglio, R. Ornelas, F. Matteucci, J. Ledesma-Garcia, L.G. Arriaga, A.S. Arico, Electrochim. Acta 53 (2008) 7350–7356.
[22] H. Su, B.J. Bladergroen, V. Linkov, S. Pasupathi, S. Ji, Int. J. Hydrogen Energy 36 (2011) 15081–15088.
[23] E. Slavcheva, I. Radev, S. Bliznakov, G. Topalov, P. Andreev, E. Budevski, Electrochim. Acta 52 (2007) 3889–3894.
[24] E. Slavcheva, I. Radev, G. Topalov, E. Budevski, Electrochim. Acta 53 (2007) 362–368.
[25] F.M. Sapountzi, S.C. Divane, E.I. Papaioannou, S. Souentie, C.G. Vayenas, J. Electroanal. Chem. 662 (2011) 116–122.
[26] K. Kadakia, M.K. Datta, O.I. Velikokhatnyi, P. Jampani, S.K. Park, P. Saha, J.A. Poston, A. Manivannan, P.N. Kumta, Int. J. Hydrogen Energy 37 (2012) 3001–3013.
[27] A. Marshall, B. Børresen, G. Hagen, M. Tsypkin, R. Tunold, Electrochim. Acta 51 (2006) 3161–3167.
[28] A. Marshall, S. Sunde, M. Tsypkin, R. Tunold, Int. J. Hydrogen Energy 32 (2007) 2320–2324.
[29] C.P. De Pauli, S. Trasatti, J. Electroanal. Chem. 538-539 (2002) 145–151.
[30] F. Fouda-Onana, N. Guillet, A.M. AlMayouf, J. Power Sources 271 (2014) 401–405.
[31] H. Kim, N.P. Subramanian, B.N. Popov, J. Power Sources 138 (2004) 14–24.
[32] S.H. Ahn, B.-S. Lee, I. Choi, S.J. Yoo, H.-J. Kim, E. Cho, D. Henkensmeier, S.W. Nam, S.-K. Kim, J.H. Jang, Appl. Catal. B: Environ. 154–155 (2014) 197–205.
[33] K. Yamanaka, Jpn. J. Appl. Phys. 28 (1989) 632–637.
[34] J. Yano, K. Noguchi, S. Yamasaki, S. Yamazaki, Electrochem. Commun. 6 (2004) 110–114.
[35] C. Terashima, T.N. Rao, B.V. Sarada, N. Spataru, A. Fujishima, J. Electroanal. Chem. 544 (2003) 65–74.
[36] E. Prats-Alfonso, L. Abad, N. Casan-Pastor, J. Gonzalo-Ruiz, E. Baldrich, Biosens. Bioelectron. 39 (2013) 163–169.
[37] J.M. Zhang, C.J. Lin, Z.D. Feng, Z.W. Tian, J. Electroanal. Chem. 452 (1998) 235–240.
[38] I.A. Ges, B.L. Ivanov, A.A. Werdich, F.J. Baudenbacher, Biosens. Bioelectron. 22 (2007) 1303–1310.
[39] P. Steegstra, E. Ahlberg, Electrochim. Acta 76 (2012) 26–33.
[40] T.Y. Kim, S. Yang, Sen. Actuators B: Chem. 196 (2014) 31–38.
[41] K. Paztor, A. Sekiguchi, N. Shimo, N. Kitamura, H. Masuhara, Sen. Actuators B 12 (1993) 225–230.
[42] M. Wang, Z. Wang, X. Gong, Z. Guo, Renewable Sustainable Energy Rev. 29 (2014) 573–588.
[43] M. Hara, K. Asami, K. Hashimoto, T. Masumoto, Electrochim. Acta 28 (1983) 1073–1081.
[44] S. Le Vot, L. Roué, D. Bélanger, Electrochim. Acta 59 (2012) 49–56.
[45] Du Xianlong, Liu Yongmei, Wang Jianqiang, Cao Yong, F. Kangnian, Chin. J. Catal. 34 (2013) 993–1001.
[46] C.D. Wagner, Physical Electronics Division, Perkin Elmer Corp. (1979).
[47] S.C. Mailley, M. Hyland, P. Mailley, J.M. McLaughlin, E.T. McAdams, Mat. Sci. Eng. 21 (2002) 167–175.
[48] V. Birss, R. Myers, H. Angerstein-Kozlowska, B.E. Conway, J. Electrochem. Soc. 131 (1984) 1502–1510.
[49] R. Kötz, J. Electrochem. Soc. 131 (1984) 72.
[50] J. Cheng, H. Zhang, G. Chen, Y. Zhang, Electrochim. Acta 54 (2009) 6250–6256.
[51] S. Song, H. Zhang, X. Ma, Z. Shao, R.T. Baker, B. Yi, Int. J. Hydrogen Energy 33 (2008) 4955–4961.